AGU PUBLICATIONS

Geophysical Research Letters

RESEARCH LETTER
10.1002/2016GL069312

**Key Points:**
- Clay squirt stiffening effect dominates velocity variation between drained and undrained rocks
- Squirt flow between clay micropores and matrix macropores induces wave dispersion in siltstone
- Clay squirt model helps predict wave velocity in tight rock saturated with immiscible liquids

**Correspondence to:**
J. Zhao, and J. Ba,
jgzhao761215@aliyun.com

**Citation:**
Ba, J., J. Zhao, J. M. Carcione, and X. Huang (2016), Compressional wave dispersion due to rock matrix stiffening by clay squirt flow, *Geophys. Res. Lett.*, *43*, doi:10.1002/2016GL069312.

Received 17 DEC 2015
Accepted 1 JUN 2016
Accepted article online 4 JUN 2016



# Compressional wave dispersion due to rock matrix stiffening by clay squirt flow

**Jing Ba[1,2], Jianguo Zhao[3], José M. Carcione[4], and Xingxing Huang[3]**

[1]School of Earth Science and Engineering, Hohai University, Nanjing, China, [2]Department of Computational Geophysics, Xi'an Jiaotong University, Xi'an, China, [3]State Key Laboratory of Petroleum Resources and Prospecting, China University of Petroleum (Beijing), Beijing, China, [4]Istituto Nazionale di Oceanografia e di Geofisica Sperimentale, Sgonico, Italy

**Abstract** The standard Biot-Gassmann theory of poroelasticity fails to explain strong compressional wave velocity dispersion experimentally observed in 12 tight siltstone with clay-filled pores. In order to analyze and understand the results, we developed a new double-porosity model of clay squirt flow where wave-induced local fluid flow occurs between the micropores in clay aggregates and intergranular macropores. The model is validated based on the combined study of ultrasonic experiments on specimens at different saturation conditions and theoretical predictions. The presence of a sub-pore-scale structure of clay micropores contained in intergranular macropores, where the fluid does not have enough time to achieve mechanical equilibrium at ultrasonic frequencies and thus stiffens the rock matrix, provides a suitable explanation of the experimental data. Moreover, the model provides a new bound for estimating the compressional wave velocity of tight rocks saturated with two immiscible liquids. The theoretical predictions indicate that the velocity variation between gas- and liquid-saturated specimens is predominantly induced by the clay squirt stiffening effect on the rock matrix and not by fluid substitution. The effect contributes more than 90% to the variation in the porosity range of 0–5%. Thus, clay squirt flow dominates the relationships between compressional wave velocity and pore fluid in tight rocks.

## 1. Introduction

A better understanding of the variations of compressional wave velocity in porous rocks as a function of pore fluid properties is important in hydrocarbon reservoir exploration and production. However, the classical poroelasticity theory [*Gassmann*, 1951; *Biot*, 1956] still fails to explain the observed compressional wave dispersion in rocks at different saturation conditions [*Dvorkin et al.*, 1995; *King et al.*, 2000; *King and Marsden*, 2002; *David et al.*, 2013], especially in those rocks tested at low effective pressures. Most previous studies [*Mavko and Jizba*, 1991; *Dvorkin and Nur*, 1993; *Dvorkin et al.*, 1994; *Pride et al.*, 2004] have suggested that grain contact microcracks (compliant pores) should account for the observed wave dispersion and dissipation at ultrasonic frequencies, which are much softer in comparison with the rock-matrix (stiff) pores. When a compressional wave squeezes a saturated rock, the fluid within the soft cracks squirts into the stiffer pores, causing a dynamic relaxation effect for the whole rock matrix. At ultrasonic frequencies, the pore fluid does not have enough time to achieve mechanical equilibrium in each wave cycle, so the rock is "stiffened" during wave propagation. Such stiffening of the effective elastic modulus suggests that conditions are unrelaxed for local fluid flow within the pore space. The conclusion that ultrasonic measurements on various rock types sample the saturated isolated regime is emerging from various laboratory studies [*Li et al.*, 2014]. *King and Marsden* [2002] and *Winkler and McGowan* [2004] suggested that a high effective pressure in rock tests tend to close the microcracks; therefore, this squirt-flow effect is weakened, and the Biot-Gassmann (B-G) theory can yield better predictions.

Recently, we performed systematic experimental observations on a series of tight siltstone samples, collected from a tight oil stratum in northeast China. Rock tests at a confining pressure of 50 MPa show very strong velocity dispersion in these low-permeability siltstones. However, in a number of scanning electron microscope (SEM) analyses we did not obtain solid evidence for the presence of microcracks. Instead, clay particles of 10 μm size were frequently observed on the quartz/feldspar grain surfaces, connected to the main pores. A type of submicroscopic-scale heterogeneity on a scale smaller than pore size is therefore suggested. Relevant previous studies [*Best and McCann*, 1995; *Best et al.*, 2013; *Marketos and Best*, 2010] suggested that pore-filling microporous hydrate/clay contributes significantly to compressional wave attenuation in saturated rocks. Thus a "clay squirt flow" loss mechanism is a plausible explanation where passing waves compress soft clay and lead to local fluid flow between clay micropores and rock macropores. *Marketos and Best* [2010] and

**Table 1.** Tight Rock Properties

| Samples | A | B | C | D | E | F | G | H | I | J | K | L |
|---|---|---|---|---|---|---|---|---|---|---|---|---|
| Porosity (%) | 2.88 | 4.6 | 5.2 | 5.56 | 5.6 | 5.79 | 5.8 | 6.45 | 10.87 | 12.75 | 13.09 | 13.97 |
| Permeability (md) | 0.0045 | 0.38 | 0.019 | 0.011 | 0.017 | 0.035 | 0.02 | 0.097 | 0.39 | 0.17 | 0.08 | 0.084 |
| Dry density ($g/cm^3$) | 2.61 | 2.56 | 2.58 | 2.53 | 2.52 | 2.41 | 2.55 | 2.38 | 2.29 | 2.3 | 2.28 | 2.26 |
| Quartz (%) | 33.8 | 35.7 | 24.7 | - | 31.3 | 32.3 | 35.1 | 35.9 | 35.3 | 40 | 35.8 | 33.8 |
| Feldspar (%) | 36.1 | 46 | 36.3 | - | 47.1 | 59.8 | 34.9 | 45.3 | 54.1 | 53.2 | 57.6 | 59 |
| Calcite (%) | 26 | 7.8 | 15.9 | - | 17.1 | 3.2 | 18.9 | 10.8 | 3.5 | 1.2 | 0.1 | 0.3 |
| Ankerite (%) | 1.0 | 1.1 | 20.1 | - | 1.7 | 0.0 | 7.3 | 1.6 | 1.1 | 0.8 | 0.3 | 0.9 |
| Pyrite (%) | 0.3 | 1.2 | 1.1 | - | 0.5 | 0.8 | 0.8 | 0.9 | 0.5 | 0.4 | 0.7 | 0.5 |
| Clay (%) | 2.8 | 8.2 | 1.9 | - | 2.4 | 3.9 | 3 | 5.5 | 5.5 | 4.4 | 5.5 | 5.5 |

*Best et al.* [2010] applied the Biot/squirt (BISQ) theory (presented by Dvorkin and Nur in 1993 by considering the squirt flow from grain cracks based on the Biot's poroelastic framework) to experimental data for shaly sandstones. *Leurer* [1997] presented an effective grain model for clay squirt flow in clay-rich marine sediments, which was adapted by *Best et al.* [2013] for hydrate sediments. Nevertheless, for the purpose of probing into the exact dynamic process of fluid flow between clay aggregate micropores and intergranular macropores, further studies need to propose a submicroscopic double-porosity model.

We simulate the clay squirt flow process based on the dynamic equations and analyze the effect of soft clay on compressional wave propagation by comparing experimental observations with theoretical results. A new bound is also presented for estimating *P* wave velocities in a saturated rock matrix in an unrelaxed state.

## 2. Experiments and Theoretical Models

### 2.1. Laboratory Experiments

A series of laboratory experiments was performed on 12 rock samples (cylinders 25.2 mm in diameter and 50–56 mm high) that were collected from the tight oil reservoirs of the Qingshankou Formation (approximately 2 km depth), in the Daqing oilfield of northeast China. Three sets of ultrasonic *P* and *S* waves were measured for each sample at full-water, full-oil (kerosene), and full-gas (nitrogen) saturations, respectively. We used the experimental setup of *Guo et al.* [2009] at in situ conditions (confining pressure 50 MPa, pore pressure 25 MPa, and temperature 80°C).

The rock sample properties are listed in Table 1. As a type of unconventional hydrocarbon resources, these tight oil rocks can generally be defined as muddy siltstones (except for sample D, which is a silty mudstone) and are composed of small-sized grains (quartz, feldspar, and rare calcite) and clay. The rocks are well sorted and have low porosity and low permeability. A systematic SEM analysis was performed on each rock sample, which yielded no significant evidence for existing grain-contact microcracks except for some flat intergranular pores. However, soft clay was frequently observed at the grain surfaces associated with intergranular pores (Figure 1a), forming a submicroscopic porous medium. As shown in Figure 1b for a double-porosity structure, the clay with micropores inside or connected to intergranular macropores has low porosity and high compressiblity in comparison with the main rock matrix. Thus, the waves induce local fluid flow on a scale smaller than the pore size.

Partial saturation experiments were performed on the five samples with higher porosities. In the experiments with gas and water saturation, the sample was first fully saturated with water by a depressurizing method and then placed in a drying oven at more than 120°C to vary the water saturation. We achieved the best control of water saturation by weighing the sample. The sample was sealed with a rubber jacket, and the confining pressure increased to 50 MPa. Nitrogen was injected to achieve a pore pressure of up to 25 MPa. We maintained the temperature at 80°C for half an hour and began ultrasonic wave measurements. In the experiments with oil and water, the sample was fully saturated with oil and then dried to vary the oil saturation. Water was injected into the sample for pore pressure control during the experiments.

Ultrasonic compressional and shear-wave velocities ($V_P$ and $V_S$) were obtained by picking the first arrivals of waveforms (accuracy ±0.23% for $V_P$ and ±0.16% for $V_S$). Figure 1c shows $V_P$ plotted as a function of $V_S$ for all specimens, fully saturated with gas, oil, and water, for in situ conditions.

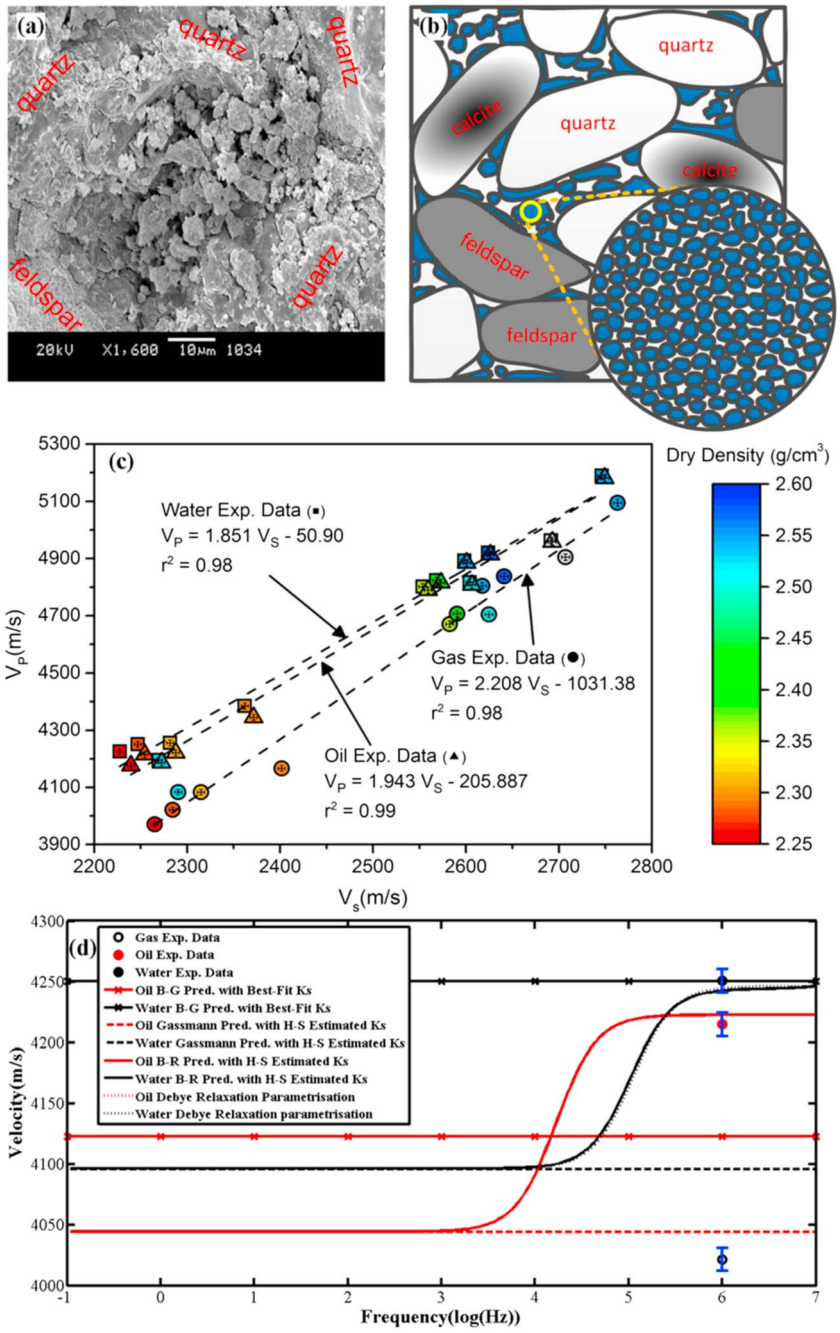


**Figure 1.** (a) SEM analyses showing clay associated with intergranular pores, forming a secondary microporous medium. (b) Schematic diagram of a submicroscopic double-porosity medium composed of intrapore clay and matrix pores. (c) Compressional wave velocity as a function of shear-wave velocity (with error bars) for 12 tight specimens at full-saturation conditions. (d) Measured compressional wave velocities in sample K (with error bars) compared with the Biot-Gassmann predictions (with a best fit mineral modulus and the Hashin-Shtrikman estimated mineral modulus, respectively) and the Biot-Rayleigh predictions (with an estimated mineral modulus); the Debye relaxation parameterization of the Biot-Rayleigh predictions is reported.

### 2.2. Biot-Gassmann Theory for Fluid Substitution

The Biot-Gassmann (B-G) theory [*Gassmann*, 1951; *Biot*, 1956] assumes that there is only one type of pore in a porous medium; thus, the same rock fully saturated with gas or fully saturated with water will share one constant matrix or frame. The theory does not consider stiffening effects, and rock's shear modulus *N* is assumed

to be independent of the pore fluid properties. The bulk modulus of the fluid-saturated rock $K_{sat}$ is related to the bulk modulus of the dry rock matrix $K_b$ (with no pore fluid) as follows

$$\frac{K_{sat}}{K_s - K_{sat}} = \frac{K_b}{K_s - K_b} + \frac{K_f}{\phi(K_s - K_f)}, \tag{1}$$

where $K_s$ is the bulk modulus of the mineral mixture, $K_f$ is the bulk modulus of the pore fluid, and $\phi$ is the porosity.

It is found that B-G theory fails to explain the experimental data for tight rock samples. As is shown in Figure 1 d for sample K, two sets of B-G predictions are compared with the measured $V_P$s. Before the predictions, the dry-rock bulk and shear moduli are determined according to the measured $V_P$ and $V_S$ at the full gas-saturation condition (the samples were dried in a drying oven under air and then velocities were measured at full nitrogen saturation). The rock porosity and density are listed in Table 1. The density, moduli, and viscosity of in situ gas, oil, and water are 0.3 g/cm$^3$, 0.089GPa, 0.031 cP and 0.79 g/cm$^3$, 1.27 GPa, 2.1 cP and 0.98 g/cm$^3$, 2.53 GPa, and 0.35 cP, respectively (determined according to *Batzle and Wang* [1992]).

In the first set of predictions, $K_s$ is reasonably estimated with a Hashin-Shtrikman (H-S) bound [*Hashin and Shtrikman*, 1963] by assuming feldspar to be the host mineral (mineral contents are listed in Table 1). However, B-G fluid substitution obviously underestimates $V_P$s in both liquid-saturation cases at a measurement frequency of 1 MHz. In the second set, $K_s$ is determined by a best fit with the measured $V_P$s at full gas- and full water-saturation conditions, based on which we try to predict the $V_P$ at full-oil saturation. It can be seen in Figure 1d that this prediction fails.

### 2.3. Biot-Rayleigh Theory for Submicroscopic Heterogeneity

The rock matrix exhibits relaxed features when saturated with gas, because of the low density, low modulus, and low viscosity of gas. Liquid saturation stiffens the rock matrix in high-frequency wave oscillations, where the fluid pressure will not achieve equilibrium because of the high fluid viscosity and fabric heterogeneity. For low-permeability rocks, the B-G theory ignores the microporosity heterogeneity and the stiffening effect induced by the inhibition of squirt flow. As is illustrated in Figure 1b, pore-related microporous clay is much softer than the host-rock matrix (which is composed of quartz/feldspar grains). Compressional waves will induce fluid pressure gradients between the clay micropores and macropores. The squirt flow process occurs sufficiently to achieve pressure equilibrium and rock relaxation in the gas saturation case.

Based on a sub-pore-scale double-porosity structure, the clay and siltstone matrices can exactly be described with the Biot-Rayleigh (B-R) theory [*Ba et al.*, 2011], which was presented to include mesoscopic heterogeneities. The governing equations for wave propagation are

$$\begin{aligned} N\nabla^2\mathbf{u} + (A+N)\nabla\varepsilon + Q_1\nabla\left(\zeta^{(1)} + \phi_2\varsigma\right) + Q_2\nabla\left(\zeta^{(2)} - \phi_1\varsigma\right) \\ = \rho_{11}\ddot{\mathbf{u}} + \rho_{12}\ddot{\mathbf{U}}^{(1)} + \rho_{13}\ddot{\mathbf{U}}^{(2)} + b_1\left(\dot{\mathbf{u}} - \dot{\mathbf{U}}^{(1)}\right) + b_2\left(\dot{\mathbf{u}} - \dot{\mathbf{U}}^{(2)}\right), \end{aligned} \tag{2a}$$

$$Q_1\nabla\varepsilon + R_1\nabla\left(\zeta^{(1)} + \phi_2\varsigma\right) = \rho_{12}\ddot{\mathbf{u}} + \rho_{22}\ddot{\mathbf{U}}^{(1)} - b_1\left(\dot{\mathbf{u}} - \dot{\mathbf{U}}^{(1)}\right), \tag{2b}$$

$$Q_2\nabla\varepsilon + R_2\nabla\left(\zeta^{(2)} - \phi_1\varsigma\right) = \rho_{13}\ddot{\mathbf{u}} + \rho_{33}\ddot{\mathbf{U}}^{(2)} - b_2\left(\dot{\mathbf{u}} - \dot{\mathbf{U}}^{(2)}\right), \tag{2c}$$

$$\begin{aligned} \phi_2\left(Q_1\varepsilon + R_1\left(\zeta^{(1)} + \phi_2\varsigma\right)\right) - \phi_1\left(Q_2\varepsilon + R_2\left(\zeta^{(2)} - \phi_1\varsigma\right)\right) \\ = \frac{1}{3}\rho_f\ddot{\varsigma}R_0^2\frac{\phi_1^2\phi_2\phi_{20}}{\phi_{10}} + \frac{1}{3}\frac{\eta\phi_1^2\phi_2\phi_{20}}{\kappa_1}\dot{\varsigma}R_0^2, \end{aligned} \tag{2d}$$

where $\mathbf{u}$, $\mathbf{U}^{(1)}$, and $\mathbf{U}^{(2)}$ are the particle displacements of the rock frame, fluid in main macropores, and fluid in clay micropores, respectively, and $e$, $\xi^{(1)}$, and $\xi^{(2)}$ are the corresponding displacement divergence fields. The scalar $\varsigma$ represents the variation of fluid content in squirt flow. Parameters $\phi_{10}$ and $\phi_{20}$ are the absolute porosities of the intergranular macropores and pore-related clay, respectively. Parameters $\phi_1$ and $\phi_2$ are the corresponding relative porosities ($\phi = \phi_1 + \phi_2$ is the rock porosity). It is assumed that the clay is homogeneously distributed in the tight rock with a volume content $v_{Clay}$; thus, the volume ratio of pore-related clay is approximately $v_{PR\text{-}Clay} = v_{Clay}\phi$, then $\phi_2 = v_{Clay}\phi\phi_{20}$. Parameter $\kappa_1$ is the rock permeability. Paramters $\eta$ and $\rho_f$ are the fluid viscosity and density, respectively. The clay aggregate is assumed spherical with radius $R_0$. The

stiffnesses $A$, $N$, $Q_1$, $Q_2$, $R_1$, and $R_2$; the density coefficients $\rho_{11}$, $\rho_{12}$, $\rho_{13}$, $\rho_{22}$, and $\rho_{33}$; and the Biot's dissipation coefficients $b_1$ and $b_2$ depend on the siltstone and clay properties [*Ba et al.*, 2011, 2015b].

The Christoffel equation is derived by substituting a plane $P$ wave kernel into equation (2a) [*Carcione*, 2015]. The solution yields the complex wave number $k$. Thus, the frequency-dependent bulk modulus of the rock matrix is

$$K_{\text{sat}} = \text{Re}\left[\omega^2\rho/k^2\right] - (4/3)N, \tag{3}$$

where $\omega$ is angular frequency and $\rho$ is the saturated rock density.

Figure 1d compares the experimental data with the B-G and B-R theoretical results. The rock properties of sample K are listed in Table 1. The relaxed bulk modulus of the rock matrix is determined according to the gas-saturation data. We take a clay porosity of 0.02, a clay bulk modulus of 0.75 GPa, and a clay aggregate radius on the order of 10 μm. A H-S estimated $K_s$ is used. The B-R theory is shown to be completely compatible with the B-G theory, yielding the same predictions at the low-frequency limit. The stiffening effect of the clay squirt flow is evident at ultrasonic frequencies in the two B-R curves, which provide much better predictions for the measured data at full liquid-saturations. The velocity differences between the gas- and liquid-saturated results can be attributed to two causes: fluid substitution and squirt-flow stiffening, and the latter is significant and relevant with clay in tight siltstones. Compared to the water-saturation case, stronger dispersion is observed in the oil-saturation case, and the dispersion inflexion point moves to the low frequencies since oil has a higher viscosity than water, indicating that for some frequency ranges in the sonic-ultrasonic band the wave velocity in an oil-saturated rock may exceed that of full water saturation. Oil and water have different characteristic frequencies ($f_c$) for stiffening. The dispersion behavior is amenable to a simpler parameterization by involving a Debye relaxation with appropriate unrelaxed and relaxed moduli and a characteristic frequency of 16.7 kHz/111 kHz at full-oil/full-water saturation. It is shown in Figure 1d that the Debye relaxation provides a perfect fit to the B-R model (they concur in the oil-saturation case). An effective "crack" aspect ratio $\alpha$ for the squirt flow is then determined by $f_c = K_s\alpha^3/\eta$ [*O'Connell and Budiansky*, 1977] ($\alpha = 0.00098$ and 0.001 for oil and water, respectively). The B-R model is validated because the Debye parameterization yields the same effective aspect ratio (~0.001) for the two full liquid-saturation cases.

## 3. Stiffened Rock Matrix Due to Clay Squirt Flow

### 3.1. BGH and BRH Bounds for Partially Saturated Rocks

The theoretical results are compared with the partial-saturation experimental data. The bounds of Biot-Gassmann-Wood and Biot-Gassmann-Hill (BGH) [*Toms et al.*, 2006; *Caspari et al.*, 2011], which assume isobaric and isolated conditions between the multiphase fluids, respectively, constrain the lower and upper limits of the compressional wave velocity as a function of saturation in the partially saturated rock. The relationship between $P$ wave velocity and saturation tends to approach the BGH bound in the ultrasonic band, especially for low-porosity rocks or rocks saturated with two liquids [*Müller et al.*, 2010; *Sun et al.*, 2015; *Ba et al.*, 2015b].

The BGH bound is

$$\frac{1}{K_p + (4/3)N} = \frac{S_1}{K_1 + (4/3)N} + \frac{S_2}{K_2 + (4/3)N}, \tag{4}$$

where $K_p$ is the bulk modulus of the partially saturated rock and $S_1$ and $S_2$ are the saturations of the two fluids, respectively. $K_1$ and $K_2$ are the bulk moduli of the fully saturated rock (with fluids 1 and 2, respectively), which are determined by equation (1). Similarly, another new constraint, the Biot-Rayleigh-Hill bound (BRH) can be derived if we use equation (3) to estimate the bulk modulus of the fully saturated rock, in which the stiffening effect of the clay squirt flow is included.

The muddy siltstones discussed in this paper have low permeability, which hinders the local fluid flow due to patchy-saturation and the related relaxation mechanism. Therefore, the BGH bound is a reasonable estimate of the compressional wave velocity, if the relaxation effect of the rock matrix can be neglected. Figure 2 shows comparisons between the partial-saturation experimental data and the theoretical predictions based on the independently measured/estimated rock properties (gas-saturated rock velocities, in situ fluid properties, rock porosity and permeability, mineral content, and H-S estimated mineral modulus). The pore-related clay-matrix bulk modulus is 0.6–0.8 GPa.

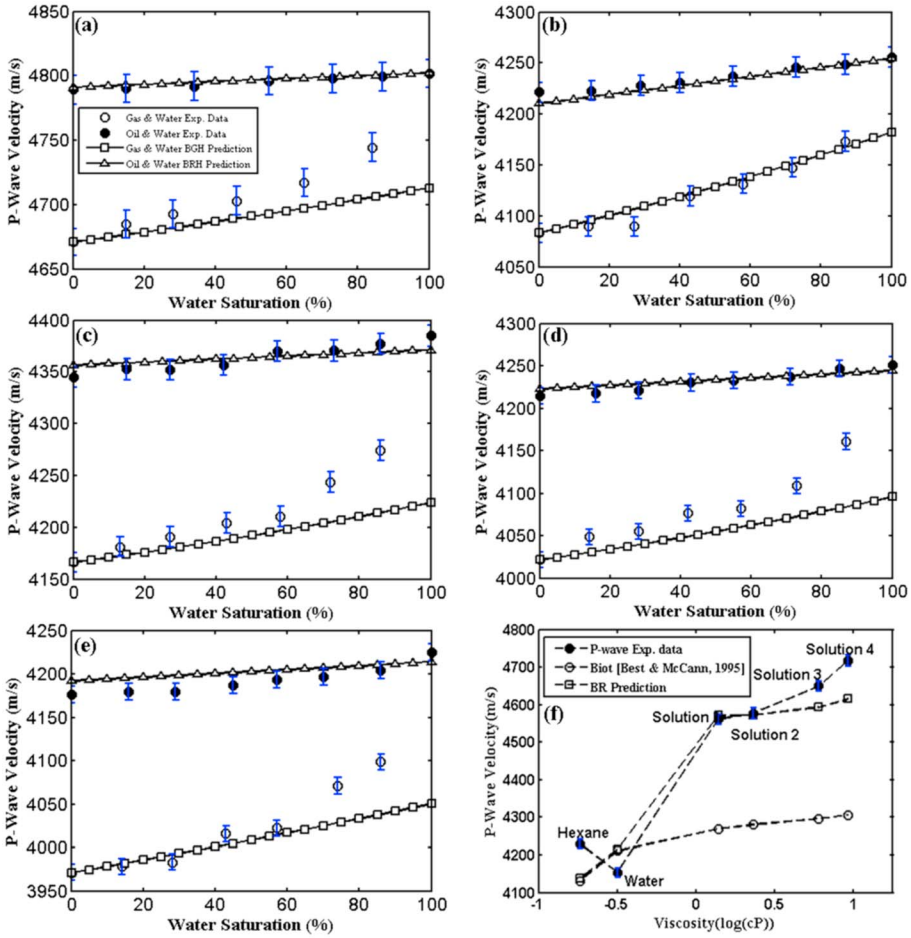


**Figure 2.** Comparisons between experimental data (with error bars) and theoretical models for compressional wave velocity as a function of water saturation in five partially saturated tight siltstones and fluid viscosity in a fully saturated shaly sandstone. (a) Sample H, (b) sample I, (c) sample J, (d) sample K, (e) sample L, and (f) York 2 shaly sandstone (data are from *Best and McCann* [1995]).

In the case of gas and water saturation, the experimental results generally agree well with the BGH bounds in the water saturation range of 0–60%. However, additional velocity dispersion is observed at high and full water saturations. When the two types of heterogeneity overlap (the first type is patchy-saturation of immiscible fluids; the second is the pore microstructure shown in Figure 1b), the first seems to dominate and suppress the latter, which supports the conclusion of a previous study [*Ba et al.*, 2015a]. Sample I (with high permeability) even shows a perfect agreement between the measurement and the BGH bound at 80% water saturation. However, at full water saturation, the B-G prediction underestimates the measurement. Low permeability may hinder the interaction of the two heterogeneities, which means that a partial stiffening effect due to clay squirt flow may still be apparent at low water saturations (see Figures 2a and 2d corresponding to samples H and K, respectively).

Unlike the relaxed state shown at full gas saturation case, there is an unrelaxed (stiffened) state in the case of oil and water partial-saturation, in which the B-G theory breaks down. The BRH prediction is based on the same set of rock parameters and shows a good agreement with the experimental data of the five samples (see Figures 2a–2e).

In Figure 2f we compare the Biot model and the clay-squirt-flow (B-R) model with the published data for York 2 sandstone [*Best and McCann*, 1995]. The shaly sandstone (porosity 13.5%, permeability 5.7 mD, clay content 20.8%, grain density 2.644 g/cm$^3$, frame bulk modulus 18.1 GPa, frame shear modulus 15.9 GPa, and grain modulus 36 GPa) was fully saturated with hexane, water, and four solutions of water and glycerol, respectively, and

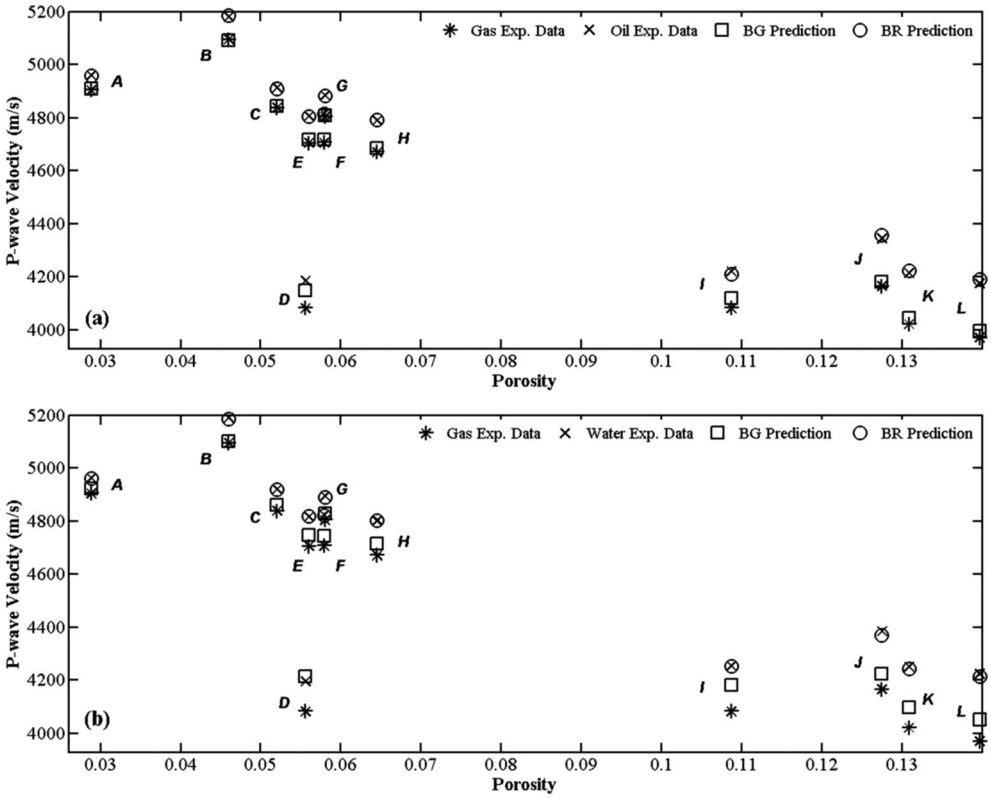


**Figure 3.** Comparisons between experimental data and theoretical predictions of compressional wave velocity as a function of porosity in (a) oil-saturated and (b) water-saturated rocks.

the ultrasonic wave velocities were measured at an effective pressure of 50 MPa and a temperature around 20°C (pore fluid properties are viscosity 0.33/1.0/23/74/456/943 cP, density 0.66/1/1.177/1.21/1.242/1.249 g/cm$^3$, and bulk modulus 0.756/2.25/3.658/3.968/4.333/4.414 GPa). We take a clay porosity of 0.02 and a clay bulk modulus of 0.4 GPa and predict the *P* wave velocities of the six cases with the same set of rock parameters by using the B-R model. The Biot theory predicts markedly lower values than the observed velocities for the four solution cases with high viscosity, whereas the B-R model gives a suitable description of the experimental data. The York 2 sandstone is a greywacke with well-sorted grains with an average diameter of 150 μm; in contrast, the siltstones measured in the present study have smaller grains (generally $<$62.5 μm) and lower permeability. The York 2 sandstone is relaxed when saturated with light liquids (hexane or water) because of its high permeability, where the B-R and Biot predictions concur. Higher viscosity of pore fluid causes the wave dispersion inflexion point to move to the low frequency band; therefore, the rock fully saturated with the solutions are unrelaxed. The B-R model gives the best description for solutions 1 and 2 while slightly underestimates the dispersion for the highly viscous fluids (solutions 3 and 4). This underestimation should be attributed to the intrinsic viscoelastic effect of the non-Newtonian fluid, which is not considered in the present model. *Marketos and Best* [2010] varied the rock parameter of the squirt-flow length of the BISQ model to achieve the best fit to the experimental data. They also concluded that the BISQ model fails to give predictions if the parameter is kept constant.

### 3.2. Stiffening Effect Versus Porosity and Clay Content

Based on the measured velocities in the 12 gas-saturated samples, the compressional velocities of the fully liquid-saturated media are predicted and illustrated in Figure 3. In general, the *P* wave velocity decreases with increasing porosity, while the velocity difference between the gas- and liquid-saturated media increases with porosity. The B-G theory fails to give appropriate predictions in almost all the specimens except for sample D, which is a silty mudstone and has an obviously lower velocity in the porosity range around 5.5%. It can be deduced that the soft clay minerals form the matrix of the rock and cannot be described by the clay-matrix double-porosity structure discussed in this work (for this case, *Best et al.* [2013] presented the Hydrate Effective Grain model, which can describe

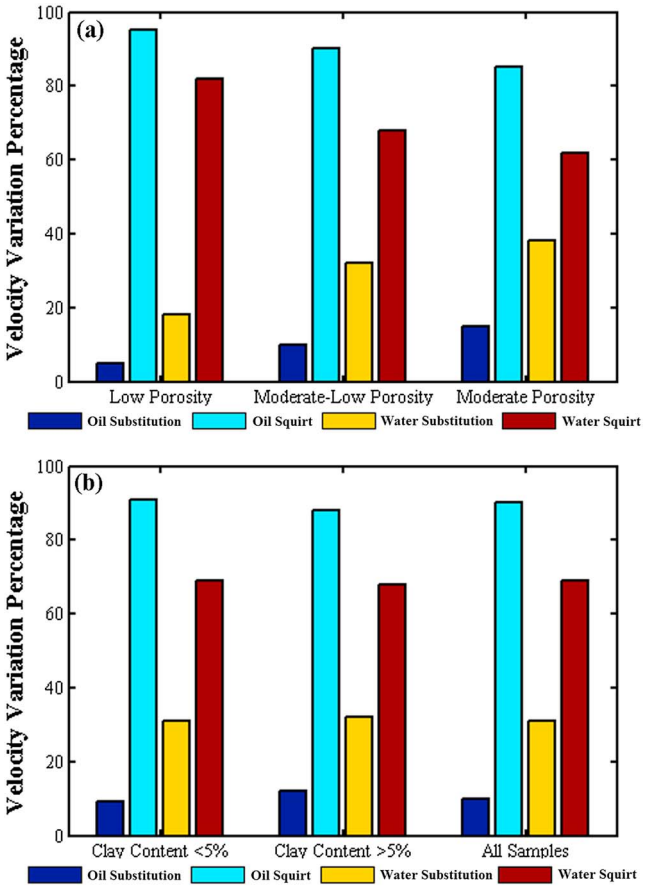


**Figure 4.** Statistical histogram of velocity variations due to different causes for (a) low porosity (<5%), moderate-low porosity (5-10%), and moderate porosity (>10%) rocks and (b) low-clay-content specimens, moderate-clay-content specimens, and all specimens.

the effect of load-bearing compliant frame minerals). The B-G theory considers the effect of fluid substitution but neglects the matrix stiffening effect of the squirt flow; thus, it underestimates the *P* wave velocity at full liquid saturation. The B-R predictions agree well with the experimental data since it includes both the fluid substitution and the squirt stiffening effects. Compared to the water-saturated case (Figure 3b), the stiffening effect is more significant for oil-saturated rocks (Figure 3a), which plays the predominant role in controlling the velocity variations between the gas-saturated and oil-saturated states.

Figure 4 shows the statistical results for the velocity variations between the gas-saturated and liquid-saturated states, due to different causes for different porosities and clay contents. In both cases, the percentage of velocity variation due to the liquid substitution increases with porosity, while that resulting from the stiffening effect of the clay squirt flow decreases (Figure 4a). Oil-saturated samples exhibit a stronger stiffening effect than water-saturated ones. In low-porosity (<5%) tight siltstones, the velocity variation due to the clay squirt flow exceeds 90% and 80% for the oil and water-saturated cases, respectively. It can be concluded that in tight reservoir rocks, the relationships between the ultrasonic *P* wave velocity and the pore fluid are dominated by the squirt flow mechanism. A similar effect can be expected at seismic and sonic frequencies if mesoscopic heterogeneity induced by clay distribution occurs in the actual strata. The effect of the B-G fluid substitution is weak, and can be neglected in the porosity range <5%. Based on compressional wave observations and measurements, oil-saturated tight rocks can hardly be discriminated from water-saturated ones in the unrelaxed state. The histograms in Figure 4b also demonstrate that the velocity variation percentage results are almost independent of the SEM-estimated clay content of the samples. The intrapore/pore-related clay induces squirt flow and matrix stiffening effects in wave oscillations; however, it cannot be directly related to the total clay content of the whole rock.

## 4. Conclusions

The effects of fluid substitution and clay squirt flow on compressional wave velocity are investigated in muddy siltstones from tight reservoirs. A comparative analysis is performed based on the ultrasonic measurements on in situ rocks and theoretical models. Strong velocity dispersion is inferred from the modeling of the difference between the measured results for gas and oil/water saturations in low-porosity specimens and the Biot-Gassmann theory fails to explain the velocity differences between different saturation regimes. Based on SEM analyses, we attribute this dispersion to a matrix stiffening effect mainly contributed by pore-filling clay. Therefore, a double-porosity structure of intrapore clay and intergranular macropores is considered. With the independently measured/estimated rock properties, the theoretical predictions of the clay squirt flow model

are in good agreement with the experimental data. In rocks partially saturated with gas and water, the Biot-Gassmann-Hill bound is able to predict the compressional wave velocity in the water-saturation range of 0–60%, suggesting that when patchy-saturation (heterogeneous distribution of immiscible fluids in low-permeability rock) and rock fabric heterogeneities (structure of clay micropores and intergranular macropores shown as illustrated in Figure 1b) coexist in specimens, the former dominates the wave propagation features. A new bound based on the clay squirt-flow model predicts the compressional wave velocity in rocks partially saturated with oil and water. Analysis at different porosities shows that the velocity variations between gas-saturated and liquid-saturated tight rocks are mainly caused by the squirt-flow stiffening effect, which decreases with increasing rock porosity.

Serial experimental measurements combined with the double-porosity model validate that the relationship between compressional wave velocity and pore fluid in tight rocks is dominated by clay squirt flow. The implications obtained from ultrasonic measurements may not be directly applicable at seismic-exploration frequencies; however, they are instructive for further seismic studies in engineering practice because larger size clay or more viscous liquid may cause stiffening effect in the seismic band. In future work, measurements on the rock samples with low-frequency laboratory techniques will be valuable in firming up the authors' interpretations. Moreover, incorporating the stiffening effect of clay squirt flow in seismic interpretation will allow the development of a multifrequency rock physics model for the target formation, where ultrasonic measurements are tied to well log data and field-observed seismic attributes and help inverting for underground rock properties and estimating fluid distributions.

**Acknowledgments**

The authors thank Ian Jackson, Angus Best, and the Editor, Bayani Cardenas, for the comments which helped improve the manuscript. This work is supported by the 973 Program of China (2014CB239006) and Natural Science Foundation of China (41274138 and 41574103). J.B. thanks Zhaobing Hao of the Institute of Geology and Geophysics, Chinese Academy of Sciences, for the help in performing experimental measurements. Data associated with this article can be accessed by contacting Jing Ba at baj04@mails.tsinghua.edu.cn.

## References

Ba, J., J. M. Carcione, and J. Nie (2011), Biot-Rayleigh theory of wave propagation in double-porosity media, *J. Geophys. Res.*, *116*, B06202, doi:10.1029/2010JB008185.

Ba, J., J. Carcione, and W. Sun (2015a), Seismic attenuation due to heterogeneities of rock fabric and fluid distribution, *Geophys. J. Int.*, *202*, 1843–1847.

Ba, J., Q. Du, J. M. Carcione, H. Zhang, and T. M. Müller (2015b), *Seismic Exploration of Hydrocarbons in Heterogeneous Reservoirs: New Theories, Methods and Applications*, Elsevier Science, Amsterdam.

Batzle, M. L., and Z. Wang (1992), Seismic properties of pore fluids, *Geophysics*, *57*, 1396–1408.

Best, A. I., and C. McCann (1995), Seismic attenuation and pore-fluid viscosity in clay-rich reservoir sandstones, *Geophysics*, *60*, 1386–1397.

Best, A. I., C. McCann, and J. Sothcott (2010), Prediction of pore fluid viscosity effects on P-wave attenuation in reservoir sandstones, in *Heavy Oils: Reservoir Characterization and Production Monitoring*, edited by S. Chopra et al., pp. 113–119, Society of Exploration Geophysicists.

Best, A. I., J. A. Priest, C. R. I. Clayton, and E. V. L. Rees (2013), The effect of methane hydrate morphology and water saturation on seismic wave attenuation in sand under shallow sub-seafloor conditions, *Earth Planet. Sci. Lett.*, *368*, 78–87.

Biot, M. A. (1956), Theory of propagation of elastic waves in fluid-saturated porous solid: II. Higher-frequency range, *J. Acoust. Soc. Am.*, *28*, 179–191.

Carcione, J. M. (2015), *Wave Fields in Real Media. Theory and Numerical Simulation of Wave Propagation in Anisotropic, Anelastic, Porous and Electromagnetic Media*, 3rd ed., Elsevier Science, Amsterdam.

Caspari, E., T. M. Müller, and B. Gurevich (2011), Time-lapse sonic logs reveal patchy $CO_2$ saturation in-situ, *Geophys. Res. Lett.*, *38*, L13301, doi:10.1029/2011GL046959.

David, E. C., J. Fortin, A. Schubnel, Y. Guéguen, and R. W. Zimmerman (2013), Laboratory measurements of low- and high-frequency elastic moduli in Fontainebleau sandstone, *Geophysics*, *78*, 369–379.

Dvorkin, J., and A. Nur (1993), Dynamic poroelasticity: A unified model with the Squirt and the Biot mechanisms, *Geophysics*, *58*, 524–533.

Dvorkin, J., R. Nolen-Hoeksema, and A. Nur (1994), The squirt-flow mechanism: Macroscopic description, *Geophysics*, *59*, 428–438.

Dvorkin, J., G. Mavko, and A. Nur (1995), Squirt flow in fully saturated rocks, *Geophysics*, *60*, 97–107.

Gassmann, F. (1951), Uber die Elastizat Poroser Medien, *Vierteljahrsschr. Naturf. Ges. Zürich*, *96*, 1–23.

Guo, M., L. Fu, and J. Ba (2009), Comparison of stress-associated coda attenuation and intrinsic attenuation from ultrasonic measurements, *Geophys. J. Int.*, *178*, 447–456.

Hashin, Z., and S. Shtrikman (1963), A variational approach to the theory of the elastic behaviour of multiphase materials, *J. Mech. Phys. Solids*, *11*, 127–140.

King, M. S., and J. R. Marsden (2002), Velocity dispersion between ultrasonic and seismic frequencies in brine-saturated reservoir sandstones, *Geophysics*, *67*, 254–258.

King, M. S., J. R. Marsden, and J. W. Dennis (2000), Biot dispersion for P- and S-wave velocities in partially and fully saturated sandstones, *Geophys. Prospect.*, *48*, 1075–1089.

Leurer, K. C. (1997), Attenuation in fine-grained marine sediments: Extension of the Biot-Stoll model by the "effective grain model" (EGM), *Geophysics*, *62*, 1465–1479.

Li, Y., M. Olin, E. C. David, I. Jackson, H. Schijns, and D. R. Schmitt (2014), Boardband laboratory measurements of dispersion in thermally cracked and fluid-saturated quartzite and a synthetic analogue, *Lead. Edge*, *33*, 624–632.

Marketos, G., and A. I. Best (2010), Application of the BISQ model to clay squirt flow in reservoir sandstones, *J. Geophys. Res.*, *115*, B06209, doi:10.1029/2009JB006495.

Mavko, G. M., and D. Jizba (1991), Estimating grain-scale fluid effects on velocity dispersion in rocks, *Geophysics*, *56*, 1940–1949.

Müller, T. M., B. Gurevich, and M. Lebedev (2010), Seismic wave attenuation and dispersion resulting from wave-induced flow in porous rocks - A review, *Geophysics*, *75*, 75A147–75A164.

O'Connell, R. J., and B. Budiansky (1977), Viscoelastic properties of fluid-saturated cracked solids, *J. Geophys. Res.*, *82*, 5719–5735, doi:10.1029/JB082i036p05719.

Pride, S. R., J. G. Berryman, and J. M. Harris (2004), Seismic attenuation due to wave-induced flow, *J. Geophys. Res.*, *109*, B01201, doi:10.1029/2003JB002639.

Sun, W., J. Ba, T. M. Müller, J. M. Carcione, and H. Cao (2015), Comparison of P-wave attenuation models of wave-induced flow, *Geophys. Prospect.*, *63*, 378–390, doi:10.1111/1365-2478.12196.

Toms, J., T. M. Müller, R. Ciz, and B. Gurevich (2006), Comparative review of theoretical models for elastic wave attenuation and dispersion in partially saturated rocks, *Soil Dyn. Earthq. Eng.*, *26*, 548–565.

Winkler, K. W., and L. McGowan (2004), Nonlinear acoustoelastic constants of dry and saturated rocks, *J. Geophys. Res.*, *109*, B10204, doi:10.1029/2004JB003262.